



Electronic structure of the $[\text{MgO}_3]^+$ cation

A. Ben Houria, O. Yazidi, N. Jaidane, M. L. Senent, and M. Hochlaf

Citation: *J. Chem. Phys.* **136**, 024316 (2012); doi: 10.1063/1.3674164

View online: <http://dx.doi.org/10.1063/1.3674164>

View Table of Contents: <http://jcp.aip.org/resource/1/JCPSA6/v136/i2>

Published by the [American Institute of Physics](http://www.aip.org).

Additional information on *J. Chem. Phys.*

Journal Homepage: <http://jcp.aip.org/>

Journal Information: http://jcp.aip.org/about/about_the_journal

Top downloads: http://jcp.aip.org/features/most_downloaded

Information for Authors: <http://jcp.aip.org/authors>

ADVERTISEMENT



Goodfellow
metals • ceramics • polymers • composites
70,000 products
450 different materials
small quantities fast

www.goodfellowusa.com

Electronic structure of the $[\text{MgO}_3]^+$ cation

A. Ben Houria,¹ O. Yazidi,¹ N. Jaidane,¹ M. L. Senent,² and M. Hochlaf^{3,a)}

¹Laboratoire de Spectroscopie Atomique Moléculaire et Applications, Département de Physique, Faculté des Sciences de Tunis, Université de Tunis-El Manar, Le Belvédère, 1060 Tunis, Tunisia

²Departamento de Química y Física Teóricas, Instituto de Estructura de la Materia, IEM-CSIC, C/Serrano 121. 28006 Madrid, Spain

³Laboratoire Modélisation et Simulation Multi Echelle, Université Paris-Est, MSME UMR 8208 CNRS, 5 bd Descartes, 77454 Marne-la-Vallée, France

(Received 29 July 2011; accepted 12 December 2011; published online 11 January 2012)

Accurate *ab initio* calculations are performed to investigate the stable isomers of $[\text{MgO}_3]^+$ and its lowest electronic states at both molecular and asymptotic regions. The calculations are done using large basis sets and configuration interaction methods including the complete active space self-consistent field, the internally contracted multi-reference configuration interaction, the standard coupled cluster (RCCSD(T)) approaches and the newly implemented explicitly correlated coupled cluster method (RCCSD(T)-F12). The presence of three stable forms is predicted: a cyclic global minimum *c*- MgO_3^+ , which is followed by a quasi-linear isomer, *l2*- MgO_3^+ . A third isomer of C_s symmetry (*l1*- MgO_3^+) is also found. Moreover, we computed the one-dimensional cuts of the six-dimensional potential energy surfaces of the lowest doublet and quartet electronic states of $[\text{MgO}_3]^+$ along the R_{MgO} and R_{OO} stretching coordinates covering both the molecular and the asymptotic regions. These curves are used later for discussing the metastability of this cation and to propose plausible mechanisms for the $\text{Mg}^+ + \text{O}_3$ atmospherically important ion–molecule reaction and related reactive channels. © 2012 American Institute of Physics. [doi:10.1063/1.3674164]

I. INTRODUCTION

Both theoretical and experimental studies showed that ion–molecule reactions play crucial roles in the Earth (ionosphere) and in the planetary atmospheres.^{1–5} The understanding of properties of their ionized regions requires the identification of the molecular species present there and the knowledge of the relevant reaction mechanisms. These mechanisms are complex and it is hard to get such information without the help of theoretical investigations.

In the literature, ion–molecule reactions data correspond mainly to investigations of reactions where the reactants are in their electronic ground states. They are used in the atmospheric models, neglecting, hence, reactants carrying internal energy.⁶ However, recent experimental findings^{7,8} and theoretical calculations^{9–14} have demonstrated the importance of both electronically and vibrationally excited reactants on this sort of reactions, especially, the branching ratios are affected. Accordingly, the consideration of the reactivity on the electronic excited states in the models dedicated to planetary atmospheres has been suggested.

From 1972, when Ferguson established the important role of metals in the ion chemistry of the atmosphere,^{15,16} they are believed to be responsible for the night air glow and the atmospheric sporadic E phenomena, and to be catalyzing the ozone decomposition. Among the reactions tabulated in Ferguson's review, we can point out the bimolecular reactive

collisions between the MgO^+ and atomic O leading to the production of the $\text{O}_2^+ + \text{Mg}$ species and the three-body collisions $\text{Ar} + \text{O}_2 + \text{Mg}^+$ producing the triatomic MgO_2^+ superoxide cation (+ Ar). We recently treated these processes where we showed that spin-orbit, vibronic, and Renner-Teller interactions occurring between the electronic ground and excited states of the MgO_2^+ superoxide for both linear and bent structures play crucial roles during the ion–molecule reactions between $\text{O/O}^+ + \text{MgO}^+/\text{MgO}$ and $\text{O}_2^+/\text{O}_2 + \text{Mg}/\text{Mg}^+$, in addition to the intramolecular isomerization processes converting *l*- MgOO^+ into *c*- MgO_2^+ and vice versa. At low collision energies, we found that the initial orientation of the reactants might favor the formation of either bent MgO_2^+ (orthogonal collisions) or *l*- MgOO^+ (collinear collisions).¹⁷

In the present paper, state-of-the art *ab initio* calculations are performed for the identification of the stable isomers and the transition states of MgO_3^+ and for computing potential energy surfaces (PESs) of the lowest electronic states of MgO_3^+ . Then, we consider the ion–molecule reactions between $\text{MgO}^+ + \text{O}_2$, $\text{MgO}_2^+ + \text{O}$, and $\text{Mg}^+ + \text{O}_3$ and their mutual coupling channels. Previous studies^{15,16} have treated the reaction between Mg^+ and O_3 leading mostly to $\text{O}_2 + \text{MgO}^+$ or $\text{MgO}_2^+ + \text{O}$. The ion–molecule reactions given above are expected to take place along the potential energy surfaces of the electronic states of the MgO_3^+ superoxide involving all isomers of the MgO_3^+ sum formula. These reactions, their reactants and their products are important to understand the ionospheric chemistry of planetary atmospheres, where they are modifying the local and global concentrations of Mg, O, O_2 , MgO , MgO_2 , and O_3 and their respective charged species.

^{a)} Author to whom correspondence should be addressed. Electronic mail: hochlaf@univ-mlv.fr. Telephone: +33 1 60 95 73 19. Fax: +33 1 60 95 73 20.

II. COMPUTATIONAL DETAILS

In the present work, all electronic calculations were performed using the MOLPRO program suite.¹⁸ We searched for stationary points determining equilibrium geometries and a set of spectroscopic parameters (rotational constant, harmonic wavenumbers, and dipole moments) using the coupled-cluster level including perturbative treatment of triple excitations,¹⁹ the newly developed and implemented (R)CCSD(T)-F12 technique (using both F12a and F12b approximations)^{20,21} as detailed in Ref. 22, and the complete active space self-consistent field (CASSCF)^{23,24} approaches. Geometry optimizations and harmonic frequencies calculations are done using the default options as implemented in MOLPRO, in the C_1 point group. We conducted calculations for the lowest doublet and lowest quartet spin multiplicity electronic states. Several numerical problems (no convergence) were encountered when computing the quartets. Electronic difference densities are computed with the MOLPRO program and drawn with the MOLDEN interface.²⁵

Since all molecular species treated here present an open shell structure, the restricted versions of the coupled-cluster approaches (RCCSD(T) and RCCSD(T)-F12) are considered. In the standard coupled-cluster calculations, we used the correlation-consistent basis sets to treat the correlation energy of the valence electrons. We examined core-valence correlation and scalar relativistic corrections as well. For the description of the Mg and O atoms, we used the following basis sets: aug-cc-pVXZ ($X = D, T, Q$), aug-cc-pCVXZ ($X = D, T$) (where all electrons were correlated and within the frozen core approximation for core-valence correlation), and aug-cc-pVXZ-DK ($X = D, T$).^{26–29} For the RCCSD(T)-F12 computations, the cc-pVXZ-F12 ($X = D, T$) explicitly correlated basis sets by Peterson and co-workers²² in connection with the corresponding auxiliary basis sets and density fitting functions^{30–32} are used. As established in the literature, the RCCSD(T)-F12/cc-pVTZ-F12 method should lead to results as accurate as RCCSD(T)/aug-cc-pV5Z with strong reduction of computational cost, both central processing unit time and disk used.^{33–36} In the following, we will not distinguish between the RCCSD(T)-F12a or RCCSD(T)-F12b results since they are close. The RCCSD(T)-F12b data will be given by default.

For the electronic excited states calculations, the generally contracted *spdf* cc-pVQZ subset basis of Dunning were used, resulting in 184 contracted Gaussian functions.^{26,28} For the computations of the one-dimensional cuts on the six-dimensional potential energy surfaces (6D-PESs) of the lowest doublet and quartet electronic states of MgO_3^+ system, we used the CASSCF (Refs. 23 and 24) method, followed by the internally contracted multi-reference configuration interaction (MRCI) approach.^{37,38} In order to reduce the size of these calculations, the three lowest σ valence molecular orbitals were optimized but kept doubly occupied. All valence electrons were correlated. For CASSCF, the electronic states of the same spin multiplicity were averaged together. For MRCI, all configurations having a weight ≥ 0.1 in the CI expansion of the CASSCF wavefunctions were taken into account as a reference. In this work, the C_2 axis is chosen to

be the y-axis for the symmetry designation of the electronic states.

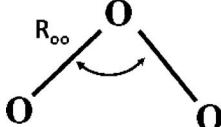
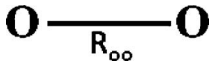
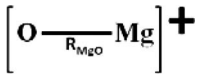
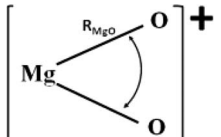
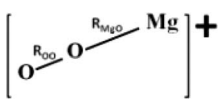
III. STABLE ISOMERS AND TRANSITION STATES OF MgO_3^+ AND FRAGMENTS

Recently, we treated the lowest electronic states of the diatomic MgO and MgO^+ and the triatomic species MgO_2^+ .^{17,39,40} For MgO_2^+ , two isomeric forms, the strongly bent form (c- MgO_2^+ \tilde{X}^2A_2) and the weakly bound *l*- $MgOO^+$ ($\tilde{X}^4\Sigma^-$) charge quadrupole complex, were described. In this new paper, their corresponding energies, structural and spectroscopic parameters, and those of the MgO_3^+ fragments (Ozone, O_2 , MgO) are given. The data obtained at the CASSCF/aug-cc-pVTZ and RCCSD(T)/aug-cc-pVQZ levels of theory are shown in Table I.

Table II presents the equilibrium geometries of the three stable isomers of MgO_3^+ computed at RCCSD(T)/aug-cc-pVXZ ($X = D, T, Q$), RCCSD(T)/aug-cc-pVXZ-DK ($X = D, T$), RCCSD(T)/aug-cc-pCVXZ ($X = D, T$) (where all electrons were correlated and within the frozen core approximation), RCCSD(T)-F12/cc-pVXZ-F12 ($X = D, T$), and CASSCF/aug-cc-pVTZ levels of theory. symmetry and spin multiplicity of the ground electronic states are also specified. The coupled-cluster approaches lead to the following order of stabilities: the most stable form is c- MgO_3^+ , followed by *l*- MgO_3^+ and then *l*l- MgO_3^+ (Table II, Figure 1). This relative order is prevented at CASSCF. In the following discussion, we will describe these three isomers and we will refer to the RCCSD(T)/aug-cc-pVQZ geometrical parameters:

- (i) c- MgO_3^+ is a cyclic isomer of C_{2v} symmetry. It corresponds to the global minimum. It possesses a ground electronic state of \tilde{X}^2B_1 nature. In the tetratomic cation, the R_{OO} distance is longer than its value in O_3 , whereas the OOO in-plane angle is reduced by $\sim 6^\circ$. The $OMgO$ angle ($\sim 90^\circ$) is distinctly larger than the one in the $OMgO^+$ cation ($\sim 43^\circ$). Therefore, the formation of c- MgO_3^+ strongly disturbs the electronic structure of the triatomic fragments. This is confirmed by the analysis of the self-consistent field (SCF) electronic density difference between the cation c- MgO_3^+ and the corresponding neutral molecule (upper trace of Figure 2). The neutral is taken at the equilibrium geometry of the cation. In this figure, the red lines correspond to the regions where the cation electron density is higher than that of the neutral molecule, and the blue lines are for the regions with a reversed situation. They illustrate how the charges are redistributed in the cationic species compared to the neutral. In addition, this figure shows that a depletion of electron density is mainly occurring in magnesium atom where the Mg atom electron density is strongly reduced in favor of the O_3 fragment. Hence, the bounding in this complex is due to charge transfer from the Mg to the O_3 moiety in concordance with a lower ionization energy of Mg ($IE(Mg) = 7.62$ eV⁴¹) and a larger ionization energy of ozone ($IE(O_3) = 12.53 \pm 0.008$ eV (Ref. 41)).

TABLE I. Electronic energies (E_h , a.u.), structural, and spectroscopic parameters of O₃, O₂, MgO⁺, and MgO₂⁺ (distances in Å, angles in degrees, fundamental frequencies in cm⁻¹, rotational constants at equilibrium in MHz, and dipole moment in Debyes).^a

	CASSCF/ aug-cc-pVTZ	RCCSD(T)/ aug-cc-pVQZ	Spectroscopic properties ^b
	\tilde{X}^1A_1 (C _{2v}) $R_{oo} = 1.250$ $OOO = 117.4^\circ$ $E_h = -224.510\ 965$	$R_{oo} = 1.243$ $OOO = 117.8^\circ$ $E_h = -225.160\ 489$	$\omega = 1147(a_1), 713(a_1), 1039(b_2)$ $A_e = 114\ 863.06,$ $B_e = 13\ 934.42$ $C_e = 12\ 426.87,$ $\mu = 0.5512$
	$X^3\Sigma_g^-$ (D _{∞h}) $R_{oo} = 1.216$ $E_h = -149.753\ 934$	$R_{oo} = 1.208$ $E_h = -150.177\ 984$	$\omega = 1577$ $B_e = 43\ 312.79$
	$X^2\Pi$ (C _{∞v}) $R_{MgO} = 1.829$ $E_h = -274.271\ 737$	$R_{MgO} = 1.828$ $E_h = -274.450\ 943$	$\omega = 719$ $B_e = 15758.01,$ $\mu = 6.6834$
	\tilde{X}^2A_2 (C _{2v}) $R_{MgO} = 1.903,$ $OMgO = 43.3$ $E_h = -349.202\ 130$	$R_{MgO} = 1.897$ $OMgO = 42.5^\circ$ $E_h = -349.585\ 088$	$\omega = 1050(a_1), 648(a_1), 623(b_2)$ $\omega = 1050(a_1), 648(a_1), 623(b_2)$ $A_e = 33419.95,$ $B_e = 11790.97$ $C_e = 8715.90,$ $\mu = 9.7719$
	$\tilde{X}^4\Sigma^-$ (C _{∞v}) $R_{MgO} = 2.839$ $R_{oo} = 1.224,$ $E_h = -349.181\ 694$	$R_{MgO} = 2.404$ $R_{oo} = 1.205$ $E_h = -349.556\ 309$	$\omega = 1590(\sigma), 119(\sigma), 46(\pi),$ $B_e = 3728.46$ $\mu = 1.1565$

^a $E(\text{Mg}^+(^2S)) = -199.371404$ a.u. (aug-cc-pVQZ); $E(\text{Mg}^+(^2S)) = -199.370461$ a.u. (aug-cc-pVTZ).^bBasis set: aug-cc-pVQZ rotational constants; aug-cc-pVTZ for ω and μ , respectively.

- (ii) The most stable isomer is followed by a quasi-linear chain structure, l2-MgO₃⁺. The nature of the electronic ground state of this complex is not obvious and depends strongly on the electronic structure treatment (electron correlation). Indeed, we calculated a doublet (\tilde{X}^2A') and a quartet (\tilde{X}^4A') which are energetically quasi-degenerate at the CASSCF level. In contrast, at the RCCSD(T) level, both electronic states are distinctly laying at 1.86 eV and 1.07 eV above c-MgO₃⁺. Since coupled-cluster approaches take *a priori* into account for a larger amount of electron correlation than CASSCF, we recommend a ground electronic state of \tilde{X}^4A' space symmetry. The doublet corresponds therefore to an electronic excited state. The SCF electronic density difference (Figure 2 middle trace) shows that we have depletion over the whole molecule and not only on the Mg atom as in (i). The central OMg bond gains electron upon complexation by charge transfer from the MgO to the OO moiety. Again, this agrees with the ionization energy ordering between O₂ and MgO (IE(MgO) = 8.0067 ± 0.0009 eV (Ref. 42), IE(O₂) = 12.07 eV (Ref. 41)).
- (iii) A *trans* chain form, l1-MgO₃⁺, located 2.15 eV above the most stable isomer. The OOO fragment really resembles to the O₃ molecule (Tables I and II). The OMg distance is relatively long ($R_{OMg} > 2.19$ Å), which reveals that this complex is formed by association of Mg⁺ and O₃ as confirmed by the electron density

diagram depicted in the lower trace of Figure 2. This trace shows -as in (ii)- a perturbation of electron density for all four atoms of the corresponding neutral species upon ionization.

Table II shows that there is convergence in the geometrical parameters as the size of the basis set increases. Scalar relativistic effects seem slightly affecting the equilibrium structures. Core valence effects lead in few cases to corrections as large as 0.01–0.02 Å for interatomic distances and to 1°–2° for in-plane angles. The inclusion of electron correlation is crucial for the description of these molecular systems. The weak bonds are more sensitive to these effects than the strong ones (e.g., external OO in l2-MgO₃⁺). For c-MgO₃⁺, the R_{MgO} is shortened by increasing the size of the basis set. This is also the case for the R_{OMg} distance of l1-MgO₃⁺ where the increase of the size of the basis set or the inclusion of the electron correlation or the inclusion of the scalar relativistic effects tend to shorten it. These effects are less crucial for the computation of the in-plane angle of c-MgO₃⁺. Whereas the OOMg angles in l2-MgO₃⁺ \tilde{X}^2A' and \tilde{X}^4A' varies by 6°–7° when computed using RCCSD(T)/aug-cc-pVXZ for X = D, T, Q or RCCSD(T)-F12 methods.

Table II gives also the harmonic wavenumbers of the three isomers computed at several levels of theory. A basis set effect is noticeable especially for the low frequency modes that need to be computed by large basis sets. For l2-MgO₃⁺ and l1-MgO₃⁺, we found strong perturbations of the frequencies revealing strong anharmonicity effects and couplings

TABLE II. Electronic energies (E_h , a.u.), structural, and spectroscopic parameters of the MgO_3^+ isomers (distances in Å; angles in degrees; and fundamental frequencies (ω_i) in cm^{-1}). θ refers to the out-of-plane torsion angle.

Method	RCCSD(T)/ aug-cc-pCVDZ				RCCSD(T)/ aug-cc-pCVTZ				RCCSD(T)-F12/ cc-pVDZ-F12			
	RCCSD(T)/ aug-cc-pVDZ	RCCSD(T)/aug- cc-pVDZ-DK	RCCSD(T)/ aug-cc-PCVDZ	All electrons were correlated	RCCSD(T)/ aug-cc-pVTZ	RCCSD(T)/ aug-cc-pVTZ-DK	RCCSD(T)/ aug-cc-pCVTZ	All electrons were correlated	RCCSD(T)/ aug-cc-pVQZ	RCCSD(T)-F12/ cc-pVDZ-F12	RCCSD(T)-F12/ cc-pVTZ-F12	CASSCF/ aug-cc- pVTZ
Isomer I: $c\text{-MgO}_3^+ \tilde{X}^2B_1 (C_{2v})^a$												
Total energy	-424.428 887	-424.364 824	-424.438 916	-424.730 017	-424.623 192	-424.550 974	-424.634 628	-425.099 912	-424.683 092	-424.698 071	-424.712 303	-424.093 278
R_{MgO}	1.959 95	1.958 36	1.955 86	1.947 99	1.945 13	1.945 13	1.940 09	1.941 51	1.939 84	1.935 08	1.934 02	1.939 84
R_{OO}	1.374 34	1.375 40	1.373 85	1.372 89	1.360 06	1.363 23	1.3608	1.359 65	1.353 71	1.353 71	1.353 71	1.380 69
$\theta_1(\text{OMgO})$	89.0	89.1	89.1	88.9	89.2	89.1	89.1	89.2	90.3	89.6	89.4	91.8
$\theta_2(\text{OOO})$	111.1	111.1	111.1	111.1	111.1	111.1	111.0	110.8	111.1	110.5	110.9	110.9
θ	0.0	0.0	0.0	0.0	0.0	0.0	0.0	0.0	0.0	0.0	0.0	0.0
$\omega_1(a_1)$	1010	1010	1013	1014	1057					1083		
$\omega_2(a_1)$	730	729	733	734	753					766		
$\omega_3(a_1)$	469	469	469	470	474					481		
$\omega_4(b_1)$	249	248	249	250	253					257		
$\omega_5(b_2)$	736	736	736	737	791					836		
$\omega_6(b_2)$	403	401	401	403	415					431		
Isomer II: $12\text{-MgO}_3^+ {}^2A' (C_s)$												
Total energy	-424.368 265	-424.304 297	-424.377 848	-424.668 269	-424.556 079	-424.483 722	-424.567 445	-425.032 584	-424.614 822	-424.622 958	-424.641 965	-424.074 962
R_{OO}	1.238 39	1.238 39	1.237 78	1.237 32	1.227 81	1.228 34	1.2276	1.231 43	1.221 99	1.225 16	1.223 05	1.222 52
R_1	2.200 64	2.201 70	2.201 43	2.190 31	2.190 06	2.187 41	2.1900	2.196 50	2.188 41	2.192 71	2.182 12	2.108 06
R_2	1.852 56	1.853 62	1.849 72	1.844 39	1.837 22	1.832 46	1.8321	1.842 40	1.8309	1.829 28	1.824 52	1.837 75
$\theta_1(\text{OOMg})$	109.3	109.2	109.3	108.4	114.7	113.6	114.6	111.2	115.5	113.3	115.3	117.0
$\theta_2(\text{OMgO})$	175.7	175.7	175.4	175.4	173.1	173.6	172.8	175.5	173.5	174.4	171.5	171.8
θ	0.0	0.0	0.0	0.0	0.0	0.0	0.0	0.0	0.0	0.0	0.0	0.0
$\omega_1(a')$	1408	1407	1408	1411	1538							
$\omega_2(a')$	724	723	725	724	734							
$\omega_3(a')$	306	305	306	315	269							
$\omega_4(a')$	121	120	121	113	129							
$\omega_5(a')$	41	41	42	51	36							
$\omega_6(a'')$	54	55	53	73	50							
Isomer II: $12\text{-MgO}_3^+ \tilde{X}^4A' (C_s)$												
Total energy	-424.408 377	-424.344 381	-424.417 938	-424.708 588	-424.595 868	-424.523 572	-424.607 216	-425.073 060	-424.654 090	-424.660 253	^b	-424.074 962
R_{OO}	1.218 82	1.218 82	1.218 1	1.216 87	1.209 82	1.209 29	1.209 47	1.208 25	1.205 06	1.207 71		1.222 52
R_1	2.147 74	2.149 33	2.151 06	2.134 68	2.120 23	2.119 17	2.120 02	2.116 81	2.117 59	2.136 63		2.108 59
R_2	1.852 03	1.852 56	1.849 24	1.844 01	1.836 16	1.836 69	1.830 81	1.831 91	1.830 87	1.828 22		1.837 75
$\theta_1(\text{OOMg})$	138.1	137.9	138.7	140.4	145.0	145.2	145.1	145.3	145.2	140.9		136.7
$\theta_2(\text{OMgO})$	176.9	176.8	178.0	179.6	177.4	177.4	177.2	177.4	176.1	177.1		171.7
θ	0.0	0.0	0.0	0.0	0.0	0.0	0.0	0.0	0.0	0.0		0.0

TABLE II. (Continued.)

Method	RCCSD(T)/ aug-cc-pCVDZ				RCCSD(T)/ aug-cc-pCVTZ				CASSCF/ aug-cc-pVTZ			
	RCCSD(T)/ aug-cc-pVDZ	RCCSD(T)/aug- cc-pVDZ-DK	RCCSD(T)/ aug-cc-PCVDZ	All electrons were correlated	RCCSD(T)/ aug-cc-pVTZ	RCCSD(T)/ aug-cc-pVTZ-DK	RCCSD(T)/ aug-cc-pCVTZ	All electrons were correlated	RCCSD(T)/ aug-cc-pVQZ	RCCSD(T)-F12/ cc-pVDZ-F12	RCCSD(T)-F12/ cc-pVTZ-F12	CASSCF/ aug-cc- pVTZ
$\omega_1(a')$	1577	1577	1578	1583	1537							
$\omega_2(a')$	723	723	725	721	733							
$\omega_3(a')$	264	265	261	260	270							
$\omega_4(a')$	145	147	134	128	130							
$\omega_5(a')$	65	68	58	45	38							
$\omega_6(a'')$	72	78	64	64	51							
Isomer III: 11-MgO ₃ ⁺ \tilde{X}^2A' (C _s) ^a												
Total energy	-424.355 735	-424.291 818	-424.365 026 3	-424.655 7854	-424.545 767 3	-424.473 494 77	-424.555 707 9	-425.022 020	-424.603 914	-424.618 831 1	-424.632 040 35	-424.036 678
R _{0mg}	2.227 62	2.228 68	2.223 56	2.212 52	2.199 58	2.198 52	2.192 08	2.188 20	2.192 71	2.222 33	2.188 47	2.192 71
R ₂	1.342 07	1.342 60	1.341 27	1.340 35	1.325 15	1.324 62	1.325 59	1.322 65	1.316 68	1.321 44	1.3188	1.333 61
R ₃	1.241 56	1.241 56	1.241 03	1.239 61	1.234 69	1.234 69	1.234 41	1.232 57	1.228 87	1.232 57	1.228 87	1.230 98
θ_1 (OOMg)	119.7	119.7	119.5	119.6	123.1	123.2	122.9	123.1	123.7	120.6	123.2	120.8
θ_2 (OOO)	115.1	115.1	115.1	115.1	115.5	115.5	115.5	115.5	115.7	115.0	115.5	115.7
θ	180.0	180.0	180.0	180.0	180.0	180.0	180.0	180.0	180.0	180.0	180.0	180.0
$\omega_1(a')$	1228	1227	1227	1233	1249	1250				1265	1270	
$\omega_2(a')$	880	878	879	885	960	961				955	971	
$\omega_3(a')$	699	699	696	703	724	726				725	733	
$\omega_4(a')$	229	229	222	237	243	244				222	245	
$\omega_5(a')$	113	113	92	100	88	90				74	113	
$\omega_6(a'')$	117	118	113	114	139	140				113	137	

^aNo convergence for the quartet at any level.^bNo convergence.

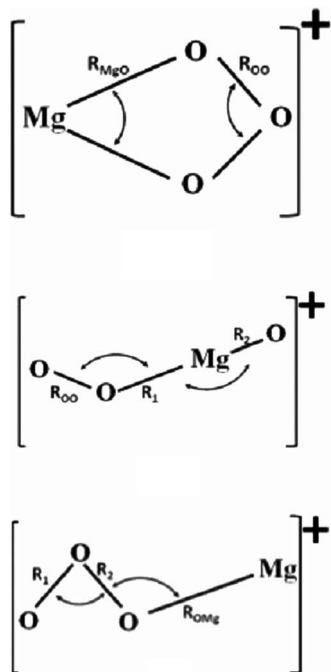


FIG. 1. Denomination of the three isomers of MgO_3^+ and definition of their internal coordinates given in Table II.

between modes. For these isomers, full six-dimensional variation calculations are needed to derive their rovibrational spectra.

For all three isomers, the MgO stretching harmonic wavenumbers are in the $725\text{--}755\text{ cm}^{-1}$ range which is laying between the MgO ($X^1\Sigma^+$) (769 cm^{-1} (Ref. 39)) and the MgO^+ ($X^2\Pi$) (719 cm^{-1} , Table I) harmonic wavenumbers. This result is consistent with a weakening of the neutral MgO bond. In the ionic tetratomic charge transfer complexes, the MgO bond should be, therefore, between MgO neutral and ionic diatomics. For $c\text{-MgO}_3^+$, we compute OOO stretchings of 1057 and 791 cm^{-1} which are lower than the corresponding harmonic wavenumbers in O_3 (1147 and 1039 cm^{-1} , Table I) as one may expect given the weakening of the OOO part upon ionization. In contrast, we compute larger O_3 wavenumbers for 11-MgO_3^+ in good agreement with the strengthening of the OOO bonds upon the formation of this molecule as expressed above. Table III lists the rotational constants at equilibrium and the dipole moment of all three isomers. The rotational constants are computed using RCCSD(T)/aug-cc-pVQZ, whereas dipole moments have been determined with CASSCF/aug-cc-pVTZ. Our calculations predict large dipole moments for isomers I and II of >9 and $>16\text{ D}$, respectively.

Additionally, we found two transition states of C_{2v} geometry, namely OMgO_2^+ (ET1) and MgOO_2^+ (ET2) (Table IV), where one central atom is linked to three atoms. They are located at 1.92 eV and 2.76 eV , respectively, over the most stable structure. Both structures show one imaginary frequency. At the RCCSD(T)/aug-cc-pVTZ level of theory, the imaginary frequency for ET1 (OMgO_2^+) is $20i\text{ cm}^{-1}$. It also possesses a low frequency mode (of 12 cm^{-1}). Strictly speaking, these values are too low and may change upon the electron correlation treatment and the basis set used for the

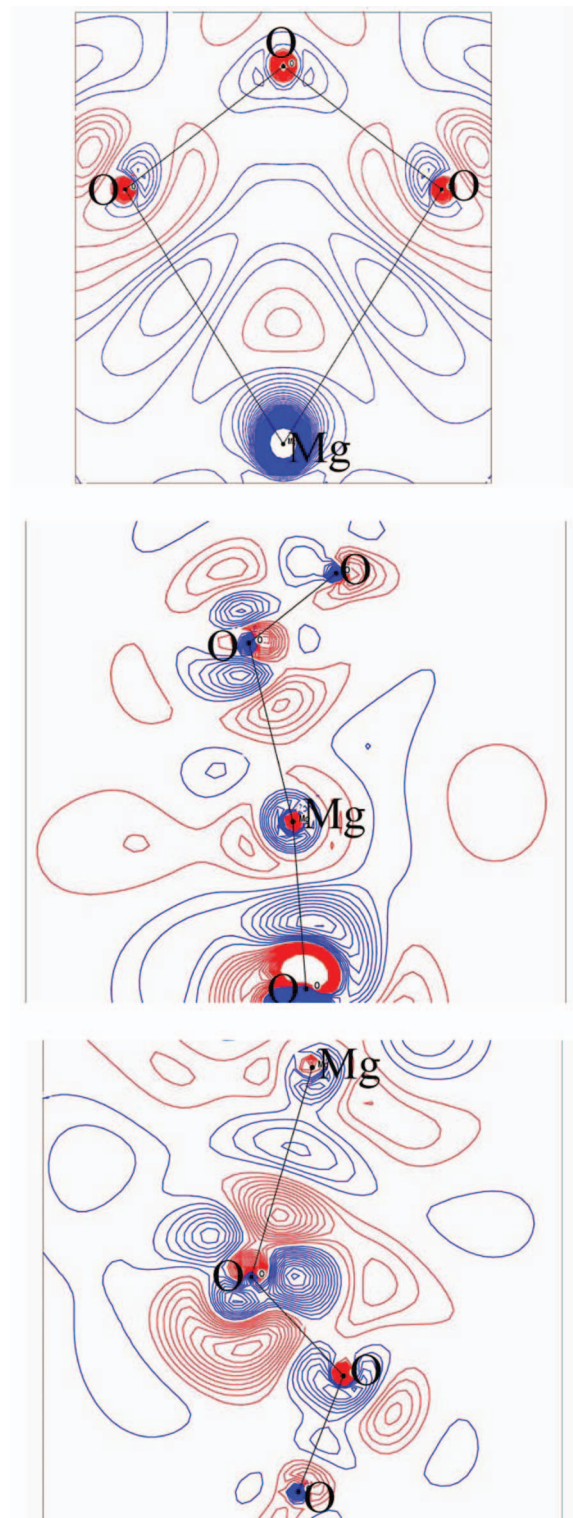


FIG. 2. SCF electronic density difference ($\Delta\rho = \rho_{\text{MgO}_3} - \rho_{\text{MgO}_3^+}$) for the equilibrium geometry of the $c\text{-MgO}_3^+$, 12-MgO_3^+ , and 11-MgO_3^+ isomers, respectively, blue lines correspond to $\Delta\rho > 0$ and red lines for $\Delta\rho < 0$. The step between the contours is 0.02 e/bohrs^3 .

description of O and Mg atoms (larger basis sets than aug-cc-pVTZ). Therefore, the exact nature of this complex, either stable or transition state, may change accordingly. Such calculations are out of the capacities of the present available computational resources and it should be confirmed in the future.

TABLE III. RCCSD(T)/aug-cc-pVQZ rotational constants at equilibrium (in MHz) and RCCSD(T)/aug-cc-pVTZ dipole moment (μ in Debye) of the stable isomers of MgO₃⁺.

Isomer	Rotational constants	μ
c-MgO ₃ ⁺ \tilde{X}^2B_1	$A_e = 127\,668.14$ $B_e = 8553.54$ $C_e = 5034.03$	$\mu = 9.2678$
12-MgO ₃ ⁺ $^2A'$	$A_e = 45\,006.72$ $B_e = 2353.00$ $C_e = 2236.09$	$\mu = 16.2942$
12-MgO ₃ ⁺ \tilde{X}^4A'	$A_e = 139\,223.20$ $B_e = 2102.41$ $C_e = 2071.13$	$\mu = 16.2906$
11-MgO ₃ ⁺ \tilde{X}^2A'	$A_e = 78\,467.26$ $B_e = 2592.08$ $C_e = 2509.19$	$\mu = 4.6370$

ET1 connects 12-MgO₃⁺ and O + c-MgO₂⁺. ET2 connects O₃ + Mg⁺ and O₂ + MgO⁺.

IV. ON THE EXCITED STATES OF MgO₃⁺ SPECIES

The reactions discussed below are *a priori* occurring along the potential energy surfaces of the electronic states of MgO₃⁺ isomers. We will start our analysis with a succinct description of the main features of these electronic states.

For c-MgO₃⁺, we depict in Figure 3 the one-dimensional cuts of its lowest electronic states along the R_{MgO} distance, where the Mg approaches the OOO part along the C_{2v} axis and for planar configuration. Figure S1 (see supplementary material⁴³) shows the cuts where the O atom approaches the OMgO triatomic. These cuts are given in energy with respect to c-MgO₃⁺ (\tilde{X}^2B_1) minimum. The cuts in Figure S1 are mainly repulsive in nature, the ones in Figure 3 present shallow (e.g., 1²A₁ and 1²B₂ curves) or deep potentials such as

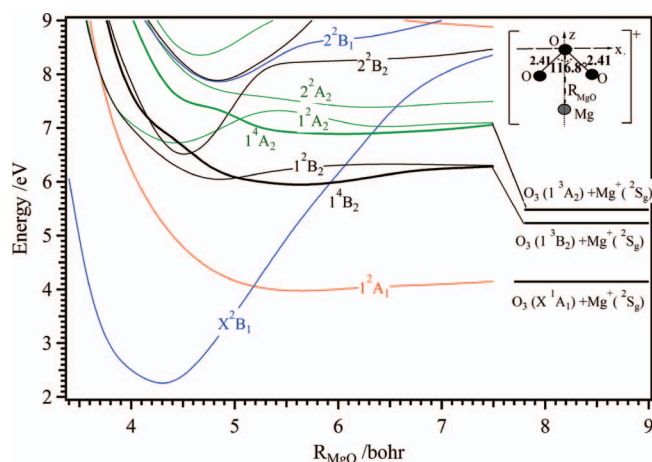


FIG. 3. MRCI potential energy curves of the lowest electronic states of [MgO₃]⁺, when the Mg⁺ atom is colliding with O₃ for bent structures. The energies are given with respect to the global minimum c-MgO₃⁺ (\tilde{X}^2B_1).

the \tilde{X}^2B_1 potential. The later one, correlates to the O₃(1³A₂) + Mg⁺(²S_g) excited asymptote and it is crossed by several other electronic states that converge to the lowest dissociation limits. At these crossings, spin-orbit conversion processes, which are of great importance for the reactive collisions between Mg/Mg⁺ and O₃⁺/O₃ may occur.

We present in Figures S2 and S3, the collinear one-dimensional cuts of the 6D-PESs of the 12-MgO₃⁺ charge transfer complex along the external and the central MgO (R_{MgO}) distance, respectively. A high density of electronic states can be seen that may favor their couplings by spin-orbit and vibronic couplings (see Ref. 43 for more details). Figure S4 displays the MRCI one-dimensional evolution of 12-MgO₃⁺ electronic states along the *cis* and *trans* bending coordinates. This figure shows that all doubly degenerate electronic states at linearity split into two components because of Renner-Teller effect. This results on additional couplings (non-adiabatic couplings) between these electronic

TABLE IV. Electronic energies (E_h , a.u.), structural, and spectroscopic parameters of the MgO₃⁺ transition states (distances in Å, angles in degrees, fundamental frequencies in cm⁻¹, rotational constants in MHz, and dipole moment in Debyes). Relative energies (E_r , eV) are given with respect to c-MgO₃⁺ (\tilde{X}^2B_1) energy at equilibrium.

	CASSCF/ aug-cc-pVTZ	RCCSD(T)/ aug-cc-pVQZ	Spectroscopic properties ^a
<p>ET1</p>	\tilde{X}^2B_2 (C _{2v}) $R_1 = 1.908$, $R_2 = 2.195$ OMgO = 158.7° $E_h = -424.057\,835$ $E_r = 0.96$	$R_1 = 1.831$, $R_2 = 2.221$ OMgO = 163.8° $E_h = -424.612657$ $E_r = 1.92$	$\omega = 1060(a_1), 664(a_1), 286(a_1), 12(b_1), 739(b_2), 20i(b_2)$ A = 41123.68, B = 2838.46 C = 2655.19, $\mu = 7.7006$
<p>ET2</p>	\tilde{X}^2A_1 (C _{2v}) MgOO = 114.9° $E_h = -423.940\,990$ $E_r = 4.14$	$R_1 = 2.931$, $R_2 = 1.273$ MgOO = 120.7° $E_h = -424.581\,832$ $E_r = 2.76$	$\omega = 1041(a_1), 622(a_1), 351(a_1), 678(b_2), 287i(b_1), 459i(b_2)$ A = 13180.73, B = 2724.93 C = 2258.10, $\mu = 14.4410$

^aBasis set: aug-cc-pVQZ rotational constants; aug-cc-pVTZ for ω and μ .

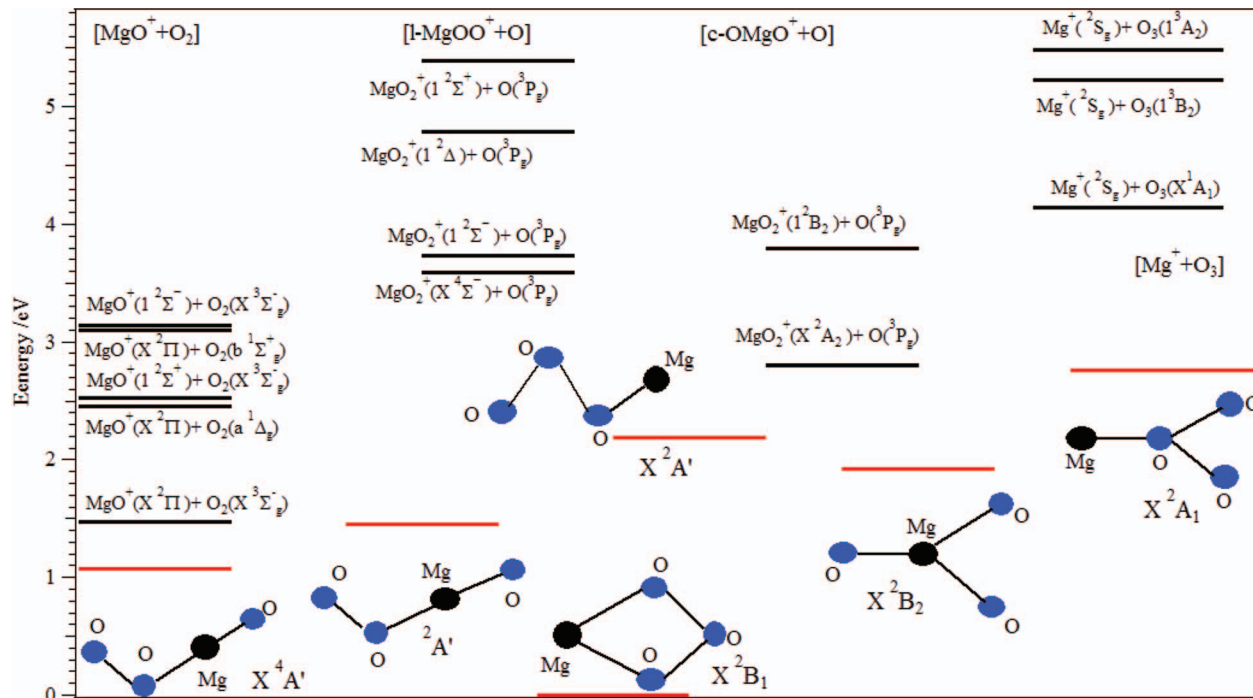


FIG. 4. Energetic diagram of the lowest dissociation limits of the MgO_3^+ cation. The energies are given with respect to the global minimum $\text{c-MgO}_3^+(\tilde{X}^2B_1)$.

states for bent structures. In addition, one can see there that the $l\text{-MgO}_3^+(\tilde{X}^2\Pi)$ state evolves to the *trans* bent $^2A'$ structure, where stable $l\text{-MgO}_3^+$ ions may be found.

Finally, we present in Figures S5–S7, the evolution of the electronic states of MgO_3^+ and OMgO_2^+ structures. Despite that these structures correspond to transition states, these cuts are important for discussing the collisions between $\text{MgO}_2/\text{MgO}_2^+ + \text{O}^+/\text{O}$ and $\text{O}_3/\text{O}_3^+ + \text{Mg}^+/\text{Mg}$. Briefly, we find some local minima (either deep or shallow) where electronically excited MgO_3^+ species may exit or evolve to the stable forms of this cation. Again, a high density of electronic states is found. These electronic states should be coupled mutually by vibronic and spin-orbit.

V. COLLISIONAL PROCESSES

Figure 4 depicts the energy diagram of various isomers and dissociation limits of $[\text{MgO}_3]^+$ relative to the global minimum structure (c-MgO_3^+). Available theoretical and experimental data and ionization energies have been used.⁴¹ The MgO_3^+ cations in their electronic ground and excited states are possible intermediates of ion-molecule reactions between O^+/O and $\text{MgO}_2/\text{MgO}_2^+$, Mg^+/Mg and O_3/O_3^+ , and O_2^+/O_2 and MgO/MgO^+ . This diagram shows the high density of channels, which may complicate the theoretical studies for these reactions, and therefore, may be the origin of the lack of their theoretical treatments.

In the present paper, we discuss the role of the Mg^+ metal atomic ion on the decomposition of the ozone molecular system and their coupled channels through the analysis of three different types of processes capable of forming the tetratomic MgO_3^+ species: (a) reactions $\text{O} + \text{MgO}_2^+$; (b) $\text{O}_3 + \text{Mg}^+$; and (c) $\text{O}_2 + \text{MgO}^+$.

Since the mapping of the six-dimensional global potential energy surfaces of the electronic states of MgO_3^+ , includ-

ing molecular, charge transfer, van der Waals, and asymptotic regions is extremely computationally demanding at an accurate level of theory, suitable one-dimensional cuts are performed on the 6-D PESs of the cation lowest electronic states. Indeed, our study is based on the utilization of several internal conversion reactions involving the atomic-triatomic and diatomic-diatom species, which are taken at their equilibrium geometries when they slightly differ from those of the tetratomic complex, except for Figure 5 where all internal coordinates were relaxed. It is worth noting that the mechanisms proposed below are plausible and should probably occur.

A. Reactions between O and MgO_2^+

The reactive collisions between O and MgO_2^+ can lead to the formation of the cyclic global minimum (c-MgO_3^+) or to the quasi-linear system ($l\text{-MgO}_3^+$). The present *ab*

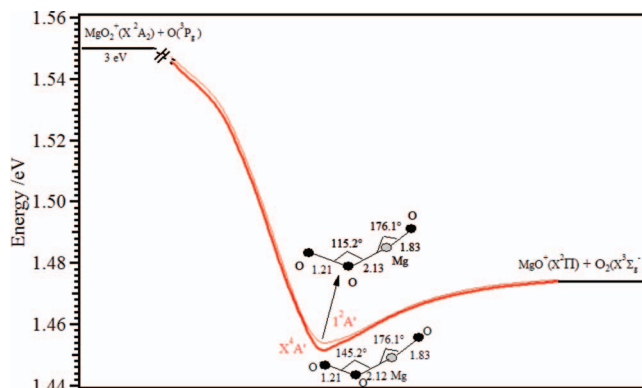


FIG. 5. MRCI minimal energy path along the lowest doublet and quartet potential energy surfaces. The energies are given with respect to the global minimum $\text{c-MgO}_3^+(\tilde{X}^2B_1)$. All coordinates were relaxed.

initio study follows three different collisional schemes: (1) The oxygen is colliding with the linear OOMg⁺ from the Mg side and along the molecular axis, which may favor the formation of the quasi-linear form l2-MgO₃⁺ (cf. Figure S2). (2) The oxygen is colliding with a bent OMgO⁺ molecule from the Mg side and along the C₂ axis (cf. Figure S5). (3) The oxygen atom is approaching the OMgO molecule for bent structures from the O's side along the C₂ axis (cf. Figure S1).

Figure 5 presents the MRCI minimal energy path for the approach of O(³P) to MgO₂⁺($\tilde{X}^4\Sigma^-$). This leads *a priori* to the formation of quasi-linear stable isomer l2-MgO₃⁺. This isomer may be dissociated thereafter by producing the same fragments O(³P) and MgO₂⁺($\tilde{X}^4\Sigma^-$). Figure S2 may be helpful for the discussion of the implication of the electronic excited states of l2-MgO₃⁺ into these reactive collisions and on the reactivity of electronically excited O and MgO₂⁺ species.

Figure S5 describes the approach of one oxygen atom O(³P) to the cyclic c-MgO₂⁺(\tilde{X}^2A_2) from the Mg side and along the C₂ axis, to form the transition state complex [O-MgO₂]⁺ in the ¹2B₂ state. This complex can dissociate later to give the same fragments (O(³P) and c-MgO₂⁺(\tilde{X}^2A_2)) following the reversed path.

Figure S1 describes the approach of oxygen O(³P) with c-MgO₂⁺(\tilde{X}^2A_2) from the O's side and along the C₂ axis. This collision may give the cyclic isomer [O₃Mg]⁺ in the unstable ¹2B₂ state, which can dissociate later to give the same fragments.

B. Reactions between MgO⁺ and O₂

Our calculations are performed for different collision schemes where the diatomic internuclear axes are either coinciding together or perpendicular to each other. In both cases, the O₂ molecule can approach MgO⁺ either by the Mg atom or by the O atom (cf. Figures 5, S3 and S7).

Figure 5 displays the minimal energy path computed at the MRCI level. This figure shows that the approach of O₂($X^3\Sigma_g^-$) to MgO⁺($X^2\Pi$) produces the l2-MgO₃⁺ isomer in its electronic ground state. This isomer dissociates giving the same fragments and back through the same path. For electronic excitation of the reactants, Figure S3 can be used where we expect the implication of several doublet and quartet electronic excited states and their mutual couplings. In Figure S7, the MgO⁺($X^2\Pi$) is pointing to the center of the O₂($X^3\Sigma_g^-$) molecule by the O atom (*orthogonal* collision scheme). This reaction produces (O-MgO₂)⁺ in the ¹2B₁ or ¹2B₂ states. The dissociation of this species occurs back through the same path.

C. Reactions between Mg⁺ and O₃

The present theoretical study of the reactive collision between Mg⁺ cation and neutral ozone follows two different collision schemes: (i) The Mg⁺ cation approaches to the O₃ molecule from the two Os sides along the C₂ axis to produce bent structures (cf. Figure 3). (ii) The Mg⁺ cation is colliding with a bent O₃ molecule from the central O side and along the C₂ axis (cf. Figure S6).

In Figure 3, the Mg⁺ cation (¹2S_g) approaches to the O₃(\tilde{X}^2A_1), leading to the cyclic isomer c-MgO₃⁺ in the dis-

sociative state ¹2A₁. By spin-orbit conversion, it may fall on the fundamental stable state \tilde{X}^2B_1 , then dissociates to give the same fragments in their ground states and back through the same path. The same figure shows how ozone in its first excited state (¹3B₂) reacts with Mg⁺(²S_g) to give the cyclic isomer c-MgO₃⁺ in an excited state (¹2B₂ or ¹4B₂). Then, it dissociates returning by the same path. In addition, the reaction of ozone in its first excited state (¹3B₂) with Mg⁺(²S_g) may give the cyclic isomer c-MgO₃⁺ in the \tilde{X}^2B_1 state after ¹2B₂/¹4B₂ → \tilde{X}^2B_1 spin-orbit conversion.

The cyclic isomer c-MgO₃⁺ in its ground state can dissociate directly to produce O₃(¹3A₂) + Mg⁺(²S_g) or, by spin-orbit conversion, to the second dissociation limit O₃(¹3B₂) + Mg⁺(²S_g) via the ²B₁ or the ¹4B₁ states. Final, this cyclic isomer can dissociate to the first dissociation limit O₃(\tilde{X}^1A_1) + Mg⁺(²S_g) by spin-orbit conversion through the ¹2A₁ state. Figure S6 proves that the Mg⁺(²S_g) cation approaching with a bent O₃(\tilde{X}^1A_1) molecule from the O side and, along the C₂ axis, leads to a non-reactive collision since the potential of the ¹2A₁ state along with this reaction occurs, is repulsive in nature.

Experimentally, Ferguson¹⁵ found that the reaction between Mg⁺ and O₃ leads to O₂ + MgO⁺. At thermal collision energies (>4.3 eV), our curves show that the colliding systems possess enough internal energy to dissociate forming the desired products. *A priori*, this reaction evolves several electronic states of the l2-MgO₃⁺ weakly bound charge transfer form and their mutual couplings. The corresponding mechanisms can be deduced using Figures S6 or S7 (after rotating the MgO moiety to fit the collinear configuration). This tetraatomic decomposes later to form hence the MgO⁺ + O₂ products via the reaction path identified in Figure 5. The implication of such weakly bound molecules rather than the strongly bound isomers was also noticed and established for the O⁺/O + CO₂/CO₂⁺ → O₂⁺/O₂ + CO/CO⁺ reactive collisions.^{12,13} Figure 6 presents a diagram that shows how the minimal structures, the transition states, and the Mg⁺ + O₃ channel are connected together. This should help in understanding the present collisional mechanisms together with our one-dimensional cuts. Mainly, it reveals the importance of the Mg⁺ cation in the ozone reactivity.

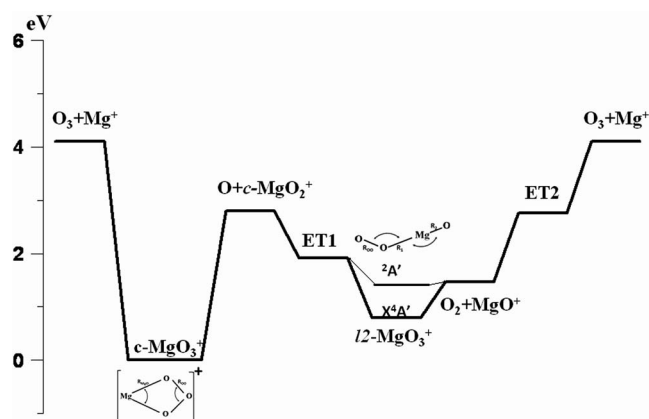


FIG. 6. Energy diagram of the MgO₃⁺ isomers, intermediates, transition states, and dissociation channels involved in the O₃ + Mg⁺ reaction. The reference energy corresponds to the c-MgO₃⁺ equilibrium energy.

VI. CONCLUSIONS

Using state-of-the-art theoretical methods, we investigate the stable isomers and transition states of MgO_3^+ which are relevant for atmospheric chemistry. These computations are performed using *ab initio* methodologies. Our calculations predict the existence of three stable isomers ordered in energy as follows: c- MgO_3^+ , l2- MgO_3^+ , and l1- MgO_3^+ .

For the charge transfer and electronic deexcitations between $\text{O}_2/\text{O}_2^+ + \text{MgO}^+/\text{MgO}$, $\text{O}/\text{O}^+ + \text{MgO}_2^+/\text{MgO}_2$, and $\text{Mg}/\text{Mg}^+ + \text{O}_3^+/\text{O}_3$, multi-step reaction pathways are discussed in light of the present theoretical data. Our calculations show that these pathways are involving both the long-range and molecular region ranges of the potential energy surfaces of the electronic states of the stable isomers of MgO_3^+ either strongly or weakly bound. According to previous theoretical and experimental works on similar ion-molecule reactions,^{44–49} the Renner-Teller and vibronic effects, together with the spin-orbit interaction should play crucial roles and participate in the mixing of the wavefunctions of these electronic states which complicate the reaction pathways undertaken. Presently, nothing is said on the efficiency of these reactive channels which can be discussed only after dynamical calculations on our 6D-PESs and their mutual couplings. Such computations are still challenging for a reactive system formed by four open shell heavy atoms and viewed the high density of electronic states and dissociation limits that should be considered and for molecular systems involving both strongly bound and weakly bound charge transfer complexes. Only calculations performed on *conventional* molecules are presented in the literature.⁵⁰

Finally, the initial orientation of the reactants, in the entrance channels, seems strongly influencing the reaction mechanisms undertaken. For instance, the collisions between $\text{Mg}^+(^2S_g)$ and $\text{O}_3(\tilde{X}^1A_1)$ molecule from the central O side lead to non-reactive collisions whereas it leads to the formation of the c- MgO_3^+ isomer when the Mg^+ is approaching the O_3 from the other side.

ACKNOWLEDGMENTS

This work has been supported by the PCI program of AECID-MAE of Spain, project PCI A/5107/06. M. L. Senent acknowledges the *Ministerio de Educación of Spain* for the grant (Grant No. AYA2008-00446 and for computing resources of CESGA. M.H. thanks a financial support from the PCMI program (INSU, CNRS).

- ¹W. R. Anderson, J. A. Vanderhoff, A. J. Kotlar, M. A. Dewilde, and R. A. Beyer, *J. Chem. Phys.* **77**, 1677 (1982).
- ²R. A. Perry, *J. Chem. Phys.* **82**, 5485 (1985).
- ³V. G. Anicich and W. T. Huntress, Jr., *Astrophys. J., Suppl.* **62**, 553 (1986).
- ⁴M. Nejad, D. A. Williams, and S. B. Charnley, *Mon. Not. Roy. Astron. Soc.* **246**, 183 (1990).
- ⁵V. G. Anicich, *Astrophys. J., Suppl.* **84**, 215 (1993).
- ⁶V. G. Anicich, *J. Phys. Chem. Ref. Data* **22**, 1469 (1993).
- ⁷C. Nicolas, C. Alcaraz, R. Thissen, J. Zabka, and O. Dutuit, *Planet. Space Sci.* **50**, 877 (2002).
- ⁸C. Alcaraz, C. Nicolas, R. Thissen, J. Zabka, and O. Dutuit, *J. Phys. Chem. A* **108**, 9998 (2004).

- ⁹M. Hochlaf, *J. Phys. Chem. A* **108**, 4978 (2004).
- ¹⁰J. Palaudoux and M. Hochlaf, *J. Chem. Phys.* **121**, 1782 (2004).
- ¹¹H. Ndome and M. Hochlaf, *Phys. Chem. Chem. Phys.* **7**, 1568 (2005).
- ¹²H. Ndome, C. Alcaraz, and M. Hochlaf, *J. Chem. Phys.* **127**, 064312 (2007).
- ¹³H. Ndome, C. Alcaraz, and M. Hochlaf, *J. Chem. Phys.* **127**, 064313 (2007).
- ¹⁴H. Ndome and M. Hochlaf, *J. Chem. Phys.* **130**, 204301 (2009).
- ¹⁵E. E. Ferguson, *Radio Sci.* **7**, 397, doi:10.1029/RS007i003p00397 (1972), and references therein.
- ¹⁶E. Murad, *J. Geophys. Res.* **83**, 5525, doi:10.1029/JA083iA12p05525 (1978), and references therein.
- ¹⁷O. Yazidi, A. Ben Houria, Z. Ben Lakhdar, M. L. Senent, and M. Hochlaf, *Chem. Phys.* **348**, 215 (2008).
- ¹⁸H.-J. Werner, P. J. Knowles, R. Lindh, F. R. Manby, M. Schütz, *et al.*, Molpro, version 2010.1 a package of *ab initio* programs, 2010, see <http://www.molpro.net>.
- ¹⁹P. J. Knowles, C. Hampel, and H.-J. Werner, *J. Chem. Phys.* **99**, 5219 (1993); **112**, 3106 (2000).
- ²⁰H. J. Werner, T. B. Adler, and F. R. Manby, *J. Chem. Phys.* **126**, 164102 (2007).
- ²¹T. B. Adler, G. Knizia, and H.-J. Werner, *J. Chem. Phys.* **127**, 221106 (2007).
- ²²K. A. Peterson, T. B. Adler, and H.-J. Werner, *J. Chem. Phys.* **128**, 084102 (2008).
- ²³P. J. Knowles and H.-J. Werner, *Chem. Phys. Lett.* **115**, 259 (1985).
- ²⁴H.-J. Werner and P. J. Knowles, *J. Chem. Phys.* **82**, 5053 (1985).
- ²⁵G. Schaftenaar and J. H. Noordik, *J. Comput.-Aided Mol. Des.* **14**, 123 (2000).
- ²⁶T. H. Dunning, *J. Chem. Phys.* **90**, 1007 (1989).
- ²⁷Unofficial set from D. Feller for Mg, see <https://bse.pnl.gov/bse/portal>.
- ²⁸D. E. Woon and T. H. Dunning, Jr. (unpublished).
- ²⁹R. A. Kendall, T. H. Dunning, Jr., and R. J. Harrison, *J. Chem. Phys.* **96**, 6796 (1992).
- ³⁰F. Weigend, *Phys. Chem. Chem. Phys.* **4**, 4285 (2002).
- ³¹C. Hättig, *Phys. Chem. Chem. Phys.* **7**, 59 (2005).
- ³²W. Klopper, *Mol. Phys.* **99**, 481 (2001).
- ³³G. Knizia, W. Li, S. Simon, and H.-J. Werner, *J. Chem. Theory Comput.* **7**, 2387 (2011).
- ³⁴V. Brites and M. Hochlaf, *J. Phys. Chem. A* **113**, 11107 (2009), and references therein.
- ³⁵F. Lique, J. Klos, and M. Hochlaf, *Phys. Chem. Chem. Phys.* **12**, 15672 (2010).
- ³⁶G. Rauhut, G. Knizia, and H.-J. Werner, *J. Chem. Phys.* **130**, 054105 (2009).
- ³⁷P. J. Knowles and H.-J. Werner, *Chem. Phys. Lett.* **145**, 514 (1988).
- ³⁸H.-J. Werner and P. J. Knowles, *J. Chem. Phys.* **89**, 5803 (1988).
- ³⁹A. Maatouk, A. Ben Houria, O. Yazidi, N. Jaidane, and M. Hochlaf, *J. Chem. Phys.* **133**, 144302 (2010).
- ⁴⁰A. Maatouk, A. Ben Houria, N. Jaidane, and M. Hochlaf, *J. Phys. B* **44**, 225101 (2011).
- ⁴¹See <http://webbook.nist.gov> for the ionisation energies.
- ⁴²D. Bellert, K. L. Burns, R. Wampler, and W. H. Breckenridge, *Chem. Phys. Lett.* **322** 41 (2000).
- ⁴³See supplementary material at <http://dx.doi.org/10.1063/1.3674164> for the description of the electronic states of MgO_3^+ species.
- ⁴⁴I. Navizet, G. Chambaud, P. Rosmus, and N. Komih, *Chem. Phys.* **329**, 251 (2006).
- ⁴⁵G. Chambaud, H. Gritli, P. Rosmus, H.-J. Werner, and P. J. Knowles, *Mol. Phys.* **98**, 1793 (2000).
- ⁴⁶H.-B. Chang, Q. Meng, M.-B. Huang, and H. Dong, *Mol. Phys.* **108**, 2137 (2010).
- ⁴⁷L. Che, Z. Ren, X. Wang, W. Dong, D. Dai, X. Wang, D. H. Zhang, X. Yang, L. Sheng, G. Li, H.-J. Werner, F. Lique, and M. H. Alexander, *Science* **317**, 1061 (2007).
- ⁴⁸M. H. Alexander, H.-J. Werner, and D. E. Manolopoulos, *J. Chem. Phys.* **109**, 5710 (1998).
- ⁴⁹R. A. Dressler, Y. Chiu, D. J. Levandier, X. N. Tang, Y. Hou, C. Chang, C. Houchins, H. Xu, and C.-Y. Ng, *J. Chem. Phys.* **125**, 132306 (2006).
- ⁵⁰D. Townsend, S. A. Lahankar, S. K. Lee, S. D. Chambreaux, A. G. Suits, X. Zhang, J. Rheinecker, L. B. Harding, and J. M. Bowman, *Science* **306**, 1158 (2004), and references therein.